coatings

MDPI

Article

Peak Cutting Force Estimation of Improved Projection Profile Method for Rock Fracturing Capacity Prediction with High Lithological Tolerance

Mingyu Duan [1,2], Lefei Shao [1,*], Qibai Huang [1], Chenlin Wang [1], Xuefeng Li [3] and Yizhe Huang [4]

[1] State Key Laboratory of Digital Manufacturing Equipment and Technology, Huazhong University of Science and Technology, Wuhan 430074, China
[2] Henan Dayou Energy Co., Ltd., Yima 472300, China
[3] School of Mechanical Engineering, Nanjing Vocational University of Industry Technologe, Nanjing 210023, China
[4] School of Mechanical Engineering, Hubei University of Technology, Wuhan 430068, China
* Correspondence: m202170399@hust.edu.cn

Abstract: Prediction of rock fracturing capacity demands particular requirements for the exploitation of mineral resources, especially for the parameter design of conical pick performance for hard rock fragmentation, which must take into account differences in rock mechanical properties. Among these parameters, the peak cutting force (PCF) is important in designing, selecting, and optimizing the cutting head of mining equipment and a cutability index of rocks. Taking high lithological tolerance as demand traction, this study proposes a theoretical model for estimating the peak cutting force of conical picks based on the improved projection profile method for which the influence of alloy head, pick body structure, and installation parameters are taken into consideration. Besides, experimental results corresponding to different numbers of rock samples are used to verify the accuracy and stability of the theoretical model. Meanwhile, the comparison of performance in cutting force estimation between this model and four other existing theoretical models is conducted. The results found that the new method has the highest correlation coefficient with the experimental results and the lowest root mean square error comparing with other models, i.e., the estimation performance of this method has high lithological tolerance when the rock type increases and the lithology changes. Consequently, the proposed peak cutting force estimation of improved projection profile method will provide a more valid and accurate prediction for rock fracturing capacity with large differences in rock mechanical properties.

Keywords: rock fracturing capacity prediction; improved projection profile method; conical picks; peak cutting force; high lithological tolerance

check for updates

Citation: Duan, M.; Shao, L.; Huang, Q.; Wang, C.; Li, X.; Huang, Y. Peak Cutting Force Estimation of Improved Projection Profile Method for Rock Fracturing Capacity Prediction with High Lithological Tolerance. *Coatings* **2022**, *12*, 1306. https://doi.org/10.3390/coatings12091306

Academic Editor: Ajay Vikram Singh

Received: 17 August 2022
Accepted: 2 September 2022
Published: 6 September 2022

Publisher's Note: MDPI stays neutral with regard to jurisdictional claims in published maps and institutional affiliations.

Copyright: © 2022 by the authors. Licensee MDPI, Basel, Switzerland. This article is an open access article distributed under the terms and conditions of the Creative Commons Attribution (CC BY) license (https://creativecommons.org/licenses/by/4.0/).

1. Introduction

With the increasing demand for predicting rock fracturing capacity due to the development of mineral resources, more attention has been paid to the influence of parameter design of conical picks on rock breaking. Accurate rock fracturing capacity prediction with high lithological tolerance is the guarantee of optimal design of conical pick parameters. Of these, peak cutting force (PCF) is not only an important parameter in designing, selecting and optimizing cutting head of mining equipment, but also an indicator of rock cutability.

In the last few decades, many researchers have done much work on rock cutting process and cutting force estimation theoretically, but little attention has been paid to the influence of lithological diversity on the stability of model predictions. Some scholars have derived their PCF estimation models based on different fracture theories during rock fracture. Evans I [1,2] firstly proposed a theoretical model for estimating the cutting force of conical picks based on the maximum tensile strength theory. Roxborough and

Liu [3] modified the model to consider the effect of friction. Goktan [4,5] introduced the parameter of rake angle to take account of asymmetrical attack, and developed a modification prediction equation on Evans' cutting theory of the peak cutting force by analyzing the full-scale rock cutting test data. Nishimatsu [6] formulated the cutting force based on the stress condition of straight envelope of Mohr's circles for brittle materials.

However, according to the research of Bilgin [7], the performance of the existing theoretical models on estimating cutting force is still unsatisfactory compared with experimental results. Therefore, many researchers have studied and revised the PCF by conducting experimental, theoretical, and numerical investigations. Tiryaki [8] developed six different empirical models based on multiple regression analysis, regression tree models, and neural network methods. Bao [9] clarified that the peak cutting force is not proportional to the square of cutting depth according to their experimental observations. Therefore, he improved the model based on the geometric similarity and energy method. Kuidong [10] established a theoretical model of PCF based on elastic fracture mechanics theory. In addition, the reliability and correctness of this model was verified by linear regression analysis. Griffith's fracture mechanics theory is established from the perspective of microcracking and crack expansion within the material, and is more applicable to anisotropic coal rock materials. Li [11–15] used the discrete element method to calculate the dynamics of the rock breakage and modeled the PCF by using the energy and stress criteria of Griffith's fracture mechanics theory. In order to clarify the rock burst process, Li [16] established three-dimensional FEM models and Wang [17–20] used a triaxial test apparatus to record the real-time values of the stresses and pick forces. Afterwards, a theoretical model for the analysis of PCF and associated factors was provided by investigating the effect of uniaxial lateral stress on rock cutability.

In summary, theoretical and empirical models for estimating the PCF of conical picks have been established by various scholars from theoretical, experimental and numerical simulation perspectives. However, the theoretical models or empirical formulas established by Evans et al. based on different rock failure criteria only considered the contribution of the alloy head structure to the PCF, ignoring the influence of the pick body on the PCF, resulting in a lack of accuracy and reliability of the theoretical model, thus making a weak correlation between the estimated and experimental values. On the other hand, the empirical model established by Bao et al. has high accuracy, but the empirical model needs a large amount of experimental support, and the high cost limits the practical application. In addition, niether model verified the influence of lithological diversity on the stability of model predictions.

To solve the problems in these existing models, an improved projection profile method is used to establish a new theoretical model for estimating peak cutting force of conical picks based on the Griffith's strength theory. The improved projection profile method is able to fully consider the effects of structural parameters including the alloy head and pick body and motion parameters including the installation angle. In addition, we present the full-scale rock cutting experimental results and four other theoretical models to verify the validity and reliability of this proposed new theoretical model. Through regression analysis and root mean square error analysis, the effects of lithology and rock sample number variations on the accuracy and stability of each theoretical model estimation are investigated.

2. Improved Projection Profile Method

The diagram of stress distribution along the tip of conical pick during the truncation process is shown in Figure 1. The parameters shown in Figure 1 are half tip angle α, taper angle of pick body α_1, radius of alloy head r, front angle β, installation angle γ and long axis of section ellipse $2a$. As an assumption, when the concentrated stress reaches the rock cracking stress, cracks will form at the pick tip. As the stress increases, the cracks propagate rapidly and lead to rock chip formation. Hence, the maximum stress appears at the pick tip while the lowest stress appears at the pick body contacting with the free surface of rock. Therefore, another assumption is that the stress decreases linearly from the pick tip to pick

body, and the direction of stress is perpendicular to the surface of the pick. The stress acting at the point C on the pick body is given by:

$$\sigma(C) = \frac{d-l}{d}\sigma_L \tag{1}$$

where l is the vertical distance from point C to pick tip, d is the cutting depth.

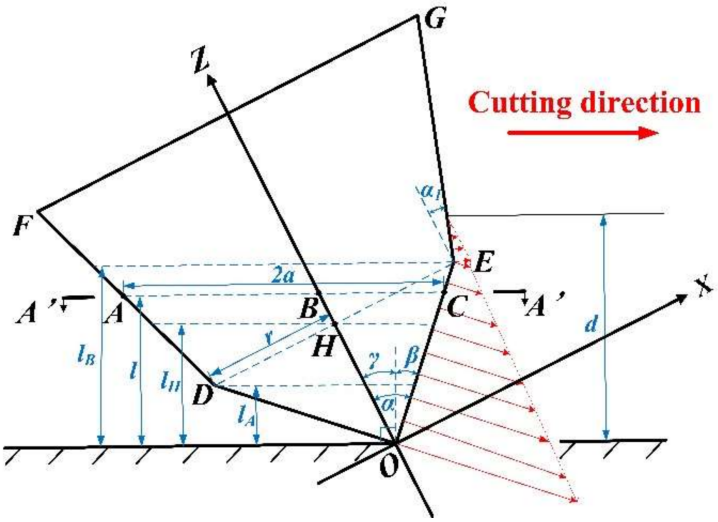

Figure 1. The diagram of the pick tip stress distribution.

According to Figure 1, projecting the alloy head and pick body profile into the XZ plane, and the generatrix equation can be given as:

$$z_{OE} = \cot(\alpha)\cdot x, 0 \le x \le r \tag{2}$$

$$z_{OD} = -\cot(\alpha)\cdot x, -r \le x < 0 \tag{3}$$

$$z_{EG} = \cot(\alpha 1)\cdot x + (\cot(\alpha)\cdot r - \cot(\alpha 1)\cdot r), x \ge r \tag{4}$$

$$z_{DF} = -\cot(\alpha 1)\cdot x + (\cot(\alpha)\cdot r - \cot(\alpha 1)\cdot r), x \le -r \tag{5}$$

When the cutting depth is l, the equation of the truncation line AC can be described as:

$$z_{AC} = -\tan(\gamma)\cdot x + l/\cos(\gamma) \tag{6}$$

By combining the equation of the pick generatrix and the truncation line, expressions of the horizontal coordinates of the points A and C corresponding to different cutting depths can be expressed as:

$$x_A = \begin{cases} \frac{l}{\cos\gamma\cdot(\tan\gamma-\cot\alpha)}, l \le l_A \\ \frac{l/\cos\gamma+(\cot\alpha 1-\cot\alpha)\cdot r}{\tan\gamma-\cot\alpha 1}, l > l_A \end{cases} \tag{7}$$

$$x_C = \begin{cases} \frac{l}{\cos\gamma\cdot(\tan\gamma+\cot\alpha)}, l \le l_B \\ \frac{l/\cos\gamma+(\cot\alpha 1-\cot\alpha)\cdot r}{\tan\gamma+\cot\alpha 1}, l > l_B \end{cases} \tag{8}$$

where $l_A = (r\cdot\cot\alpha - r\cdot\tan\gamma)\cdot\cos\gamma$, $l_B = (r\cdot\cot\alpha + r\cdot\tan\gamma)\cdot\cos\gamma$

The shape of section ABCB′ varies with the cutting depth, and its cross section is approximately elliptical. For calculation purposes, the section ABCB′ can be simplified to a circle, as shown in Figure 2.

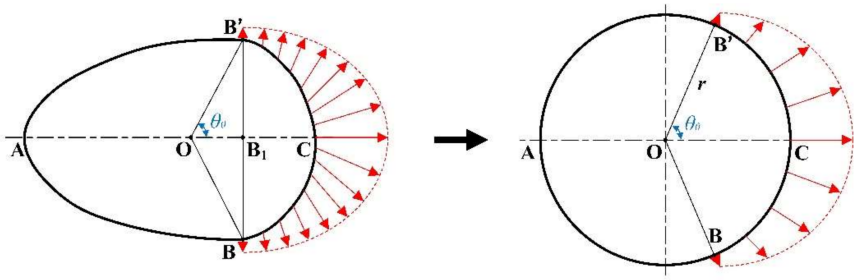

Figure 2. Section ellipse and simplified circle model.

As shown in Figure 3, AC is the long axis of the section ellipse, and the short semi-axis b corresponds to the radius r of the horizontal profile determined by the point D on the truncation line AC. The point D is determined by the horizontal coordinates of the points A and C and the correction coefficients k_1 and k_2. The long semi-axis a and short semi-axis b of the section ellipse can be expressed by the following equation.

$$\mathrm{a} = \frac{x_C - x_A}{2 \cdot \cos\gamma} \tag{9}$$

$$\mathrm{b} = \begin{cases} \frac{-\tan\gamma \cdot (x_C + k_1 \cdot x_A) + l/\cos\gamma}{\cot\alpha}, l \le l_A \\ \frac{-\tan\gamma \cdot (x_C + k_2 \cdot x_A) + l/\cos\gamma}{\cot\alpha}, l_A < l < l_H \\ \frac{-\tan\gamma \cdot (x_C + k_2 \cdot x_A) + l/\cos\gamma + (\cot\alpha 1 - \cot\alpha) \cdot r}{\cot\alpha 1}, l \ge l_H \end{cases} \tag{10}$$

where k_1 is 0.6, k_2 is 0.8, $l_\mathrm{H} = (r/\tan\alpha + \tan\gamma \cdot (x_\mathrm{C} + 0.8 \cdot x_\mathrm{A})/2) \cdot \cos\gamma$

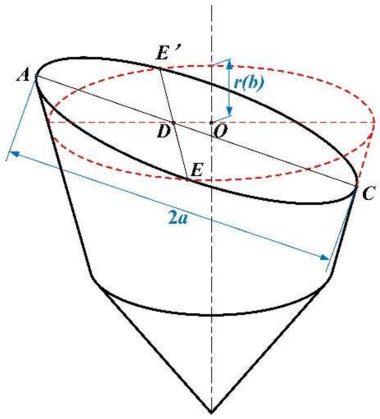

Figure 3. Schematic diagram of the long and short axes of the section ellipse.

According to the ellipse area calculation formula, the radius of the simplified circle can be expressed as:

$$\lambda = \sqrt{a \cdot b} \tag{11}$$

As shown in Figure 2, on the section of ABCB′, the cutting force only acts on the arc BCB′ which has a corresponding semi-envelope angle of θ_0. As shown in Figure 4, BB′ is the intersection line between truncation surface and vertical plane, θ_0 is the semi-envelope angle, O is the ellipse center of truncation surface ABCB′ and σ is the compressive stress on the surface of the pick, θ_0 and OB′ can be derived from the Equations (12) and (13). When the installation angle γ reaches a certain level, the long axis of the section ellipse is significantly larger than the short axis, which leads to a great increase in $|x_\mathrm{A}/x_\mathrm{C}|$. From Equation (13), this change will lead to a remarkable increase in the length of OB′, which will cause an obvious decrease in θ_0. Therefore, when the semi-envelope angle θ_0 is used to calculate the cutting force, the stress area is lower than the actual value, resulting in a smaller calculated value. To correct θ_0, the correction factor k_3 is introduced. When the

installation angle γ increases, the correction factor k_3 will decreases accordingly so that the stress area in the simplified model matches the actual one.

$$\tan\theta_0 = BB'/OB' \tag{12}$$

$$OB' = (x_C + x_A)/(2{\cdot}cos\gamma) \tag{13}$$

$$k_3 = 1 - 0.4{\cdot}\left(\left|\frac{x_A}{x_C}\right|\right) \tag{14}$$

$$\theta_0 = \begin{cases} \operatorname{atan}\left(\frac{l/\cos\gamma/\cot\alpha}{(x_C+x_A){\cdot}k_3/(2{\cdot}\cos\gamma)}\right), l \le l_A \\ \operatorname{atan}\left(\frac{l/\cos\gamma/\cot\alpha}{(x_C+x_A){\cdot}k_3/(2{\cdot}\cos\gamma)}\right), l_A < l < l_H \\ \operatorname{atan}\left(\frac{\left(\frac{l}{\cos\gamma}+(\cot\alpha_1-\cot\alpha){\cdot}r\right)/\cot\alpha_1}{(x_C+x_A){\cdot}k_3/(2{\cdot}\cos\gamma)}\right), l \ge l_H \end{cases} \tag{15}$$

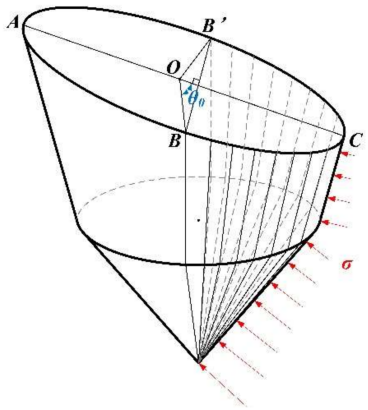

Figure 4. Schematic diagram of the force on the pick.

During the cutting process, the extrusion displacement on the section ABCB′ is perpendicular to the pick surface and decreases along point C to both sides, resulting in the stress on the section also decreasing from point C to both sides. Assuming that the stress reduction law follows a cosine distribution and is related to position angle θ, it can be expressed as:

$$\sigma = \sigma(C){\cdot}\cos\left(\frac{\theta}{\theta_0}{\cdot}\frac{\pi}{2}\right), -\theta_0 \le \theta \le \theta_0 \tag{16}$$

According to the peak stress obtained from the Griffith's theory, when the position angle is θ and the cutting depth is l, the stress can be found as:

$$\sigma = \sigma_L{\cdot}\frac{d-l}{d}{\cdot}\cos\left(\frac{\theta}{\theta_0}{\cdot}\frac{\pi}{2}\right) = \sqrt{\frac{2E\rho_S}{\pi\delta}}{\cdot}\frac{d-l}{d}{\cdot}\cos\left(\frac{\theta}{\theta_0}{\cdot}\frac{\pi}{2}\right), -\theta_0 \le \theta \le \theta_0 \tag{17}$$

where the surface energy density ρ_S of the rock can be obtained from the following equation:

$$\rho_S = \frac{K_{Ic}^2}{2E} \tag{18}$$

where K_{Ic} is the rock type I fracture toughness.

Combining the above two equations, the specific pick tip stress distribution can be given by:

$$\sigma = \frac{K_{Ic}}{\sqrt{\pi\delta}}{\cdot}\frac{d-l}{d}{\cdot}\cos\left(\frac{\theta}{\theta_0}{\cdot}\frac{\pi}{2}\right), -\theta_0 \le \theta \le \theta_0 \tag{19}$$

Equation (19) shows that the stress is negatively related to the crack size δ, as a result, the cutting force acting on the picks decreases with the expansion of the crack. Therefore,

the peak cutting force appears at the moment of crack initiation, and then decreases with crack expansion until it is reduced to a minimum when the chip is formed. This is the fundamental reason for the sawtooth-shaped change of the cutting force during the truncation process. Integrating along the contact surface between the pick and the rock, the formula for calculating the peak cutting force can be written as:

$$PCF = \int_0^d \int_{-\theta_0}^{\theta_0} \sigma \cos\varphi \cos\theta \cdot \lambda \cdot d\theta \, dl = \int_0^d \frac{K_{Ic}}{\sqrt{\pi\delta}} \cdot \frac{d-l}{d} \cdot \cos\varphi \cdot \lambda \cdot \frac{4\pi\theta_0 \cos\theta_0}{\pi^2 - 4\theta_0^2} dl \tag{20}$$

where φ is the angle between the stress perpendicular to the pick surface and the section surface, φ can be expressed as:

$$\varphi = \begin{cases} \alpha - \gamma, l \leq (r \cdot \cot\alpha + r \cdot \tan\gamma) \cdot \cos\gamma \\ \gamma - \alpha_1, l > (r \cdot \cot\alpha + r \cdot \tan\gamma) \cdot \cos\gamma \end{cases} \tag{21}$$

According to the energy criterion of Griffith's fracture theory, the energy given by the truncation process during crack extension must satisfy the surface energy required to form the new surface of the crack:

$$U_0 \geq G_S \tag{22}$$

where U_0 is the energy given by the truncation process, and G_S is the surface energy.

Assuming that the crack is a semicircle of radius δ, the surface energy required for the new surface is:

$$G_S = \pi\delta^2\gamma = \frac{\pi\delta^2 K_{Ic}^2}{2E} \tag{23}$$

Before the rock is cracked, the energy generated by the truncation process is converted into elastic energy and stored in the rock. According to the theory of linear elasticity, the work done by the truncation process can be written as:

$$U_0 = \int \Delta U dA = \int_0^d \int_{-\theta_0}^{\theta_0} \frac{\sigma^2}{2E} \cdot r d\theta \frac{dl}{\cos\varphi} = \int_0^d \frac{\left(1 - \frac{l}{d}\right)^2}{2E} \cdot \frac{K_{Ic}^2}{\pi\delta} \lambda\theta_0 \frac{dl}{\cos\varphi} \tag{24}$$

Substituting U_0 and G_S into Equation (22), the initial crack size at crack initiation can be obtained as follows:

$$\delta = \sqrt[3]{\int_0^d \frac{\left(1 - \frac{l}{d}\right)^2 \cdot \lambda\theta_0}{\pi \cdot \cos\varphi} dl} \tag{25}$$

Substituting δ into Equation (20), the peak cutting force can be expressed as:

$$PCF = \int_0^d \frac{K_{Ic}}{\sqrt{\pi \sqrt[3]{\int_0^d \frac{\left(1 - \frac{l}{d}\right)^2 \cdot \lambda\theta_0}{\pi \cdot \cos\varphi} dl}}} \cdot \frac{d-l}{d} \cdot \cos\varphi \cdot \lambda \cdot \frac{4\pi\theta_0 \cos\theta_0}{\pi^2 - 4\theta_0^2} dl \tag{26}$$

3. Validation and Discussion

The PCF calculation models need to ensure both high accuracy of cutting force prediction and high rock tolerance. In this paper, the performance of the theoretical model in predicting PCF is evaluated by analyzing the correlation between the experimental values of PCF and the theoretical calculated values. As a comparison, four other existing theoretical models are introduced in this paper, the Evans model [1] (Equation (27)), the Roxborough model [3] (Equation (28)), the Goktan semi-empirical model [4] (Equation (29)) and the Gao Kuidong model [21] (Equation (30)).

$$PCF = \frac{16\pi{\sigma_t}^2 \cdot d^2}{\cos^2\alpha \cdot \sigma_c} \tag{27}$$

where σ_t is the rock tensile strength, d is the cutting depth, σ_c is the rock uniaxial compressive strength.

$$PCF = \frac{16\pi\sigma_c d^2\sigma_t^2}{\left(2\sigma_t + (\sigma_c\cos\alpha/[(1+\tan f)/\tan\alpha])\right)^2} \tag{28}$$

where, f is the friction angle between the pick and the rock.

$$PCF = \frac{4\pi\sigma_t d^2\sin^2(\alpha+f)}{\cos(\alpha+f)} \tag{29}$$

$$\begin{cases} PCF = 2\left(\frac{\tan\alpha}{\pi E(1-\mu^2)}\right)^{\frac{1}{3}}\left(\frac{3K_{Ic}^2\tan\psi'}{k\cos\phi}\right)^{\frac{2}{3}}d^{\frac{4}{3}} \\ \psi = \pi\left(48.87 + 0.526\frac{\sigma_c}{\sigma_t}\right)/180 + 0.224\eta \end{cases} \tag{30}$$

where μ is the rock Poisson's ratio; E is therock modulus of elasticity; K_{Ic} is the rock type I fracture toughness; ϕ is the horizontal rupture angle, k is a constant related to pick shape and cutting angle, obtained by testing; ψ' is the vertical rupture angle; η is the truncation correlation coefficient, whose value is $(0.5\pi-\gamma+\alpha)/2$, where γ is the installation angle.

To verify the accuracy and stability of the PCF theoretical model proposed in this paper for different lithologies of rocks and for different numbers of rock samples, some full-scale rock cutting experimental results reported previously are cited in this section. The mechanical properties of the 27 rock samples used in these experiments [7,11,22–24] are summarized in Table 1, and these properties interact with each other during rock destruction [25–28].

Table 1. Rock mechanical properties used in cutting tests.

Group	Rock No.	Rock Type	UCS/MPa	BTS/MPa	E/GPa	ρ/kg/m^3	K_{Ic}/MPa·m$^{1/2}$
S	1	Tuff 6	6	0.2	0.4	1490	0.09
	2	Coal	3.1	0.45	4.5	1480	0.09
	3	Tuff 1	10	0.9	1.1	1490	0.21
	4	Tuff 2	11	1.2	1.4	1700	0.25
	5	Tuff 4	14	1.5	1.6	1710	0.3
	6	Tuff 5	19	2.3	1.3	1710	0.41
	7	Trona	30	2.2	3.4	2130	0.49
	8	Tuff 3	27	2.6	2.4	1800	0.51
	9	Jips	33	3	/	2320	0.59
M	10	Copper -1	33	3.4	/	4130	0.62
	11	Selestite	29	4	/	3970	0.63
	12	Chromite -1	32	3.7	3.5	4030	0.64
	13	Chromite -3	46	3.7	2.9	288	0.74
	14	Simulated coal sample	42.5	4.9	39.8	1800	0.81
	15	Chromite -2	47	4.5	2.3	3390	0.82
	16	Serpantinite	38	5.7	2.3	5490	0.82
	17	Copper -2	41	5.7	/	4070	0.85
	18	Siltstone	58	5.3	/	2650	0.96
H	19	Harsburgite	58	5.5	2.1	2650	0.97
	20	Anhydrite	82	5.5	11	2900	1.13
	21	Red Sandstone	76.3	6.6	22.4	2140	1.19
	22	Sandstone -3	87.4	8.3	33.3	2670	1.38
	23	Sandstone -1	113.6	6.6	17	2650	1.41
	24	Limestone -1	121	7.8	57	2720	1.55
	25	Limestone -2	116.4	8.2	46.3	2650	1.56
	26	Granite	161.2	8.1	1.4	2800	1.69
	27	Sandstone -2	173.7	11.6	28	2670	2.15

The samples are divided into three groups, S (soft), M (medium) and H (hard), according to the different fracture toughness of type I in Table 1. Three rock samples are selected from each group of rocks with different cutting conditions, and the predicted performance of the theoretical model is analyzed for these nine rock samples in the first analysis. The cutting parameters, i.e., pick type, cutting depth, installation angle, tip angle and the diameter of alloy head, are summarized in Table 2. The peak cutting force in different cutting conditions obtained by experiments and theoretical models are recorded in Table 3.

Table 2. Cutting conditions for the first prediction performance analysis.

Test No.	Rock No.	Pick Type	Installation Angle/°	Cutting Depth/mm	Tip Angle/°	Alloy Head Diameter/mm
1	4(S)	Sandvik 35/80H	57	5/9	80	22
2	5(S)	Sandvik 35/80H	57	5/9	80	22
3	6(S)	Sandvik 35/80H	57	5/9	80	22
4	13(M)	Sandvik 35/80H	57	5/9	80	22
5	14(M)	Sandvik 35/80H	57	5/9	80	22
6	15(M)	Sandvik 35/80H	55	10/15/20	90	22
7	22(H)	Sandvik 35/80H	57	5/9	80	22
8	23(H)	Sandvik 35/80H	57	5/9	80	22
9	24(H)	Sandvik 35/80H	57	5/9	80	22

Table 3. PCF obtained by full-scale rock cutting experiments and theoretical models for the first prediction performance analysis.

Test No.	Cut Thickness/mm	PCF_{Ex} [1]	PCF_{this} [1]	PCF_{Ev} [1]	PCF_{Ro} [1]	PCF_{Go} [1]	PCF_{Gao} [1]
1	5	7.08	1.25	0.28	0.32	1.57	1.13
	9	11.84	3.26	0.91	1.03	5.1	2.47
2	5	2.83	1.5	0.34	0.4	1.97	1.46
	9	7.3	3.91	1.12	1.28	6.37	3.19
3	5	3.44	2.05	0.6	0.64	3.02	2.72
	9	7.35	5.35	1.93	2.06	9.77	5.95
4	5	8.71	3.7	0.64	0.86	4.85	4.19
	9	16.24	9.65	2.06	2.78	15.72	9.18
5	10	30.63	16.24	5.68	4.67	27.71	6.48
	15	48.06	27.42	12.78	10.5	62.34	11.12
	20	70.12	40.99	22.72	18.66	110.84	16.32
6	5	7.85	4.1	0.92	1.13	5.9	5.69
	9	26.49	10.7	2.99	3.67	19.12	12.46
7	5	9.09	6.91	1.7	2.09	10.88	5.28
	9	15.9	18	5.49	6.76	35.26	11.57
8	5	19.69	7.06	0.82	1.27	8.65	5.47
	9	28.1	18.39	2.65	4.11	28.04	11.97
9	5	21.51	7.76	1.08	1.6	10.23	4.42
	9	29.4	20.22	3.49	5.18	33.14	9.69

[1] PCF_{Ex} is the experimental value, PCF_{This}, PCF_{Ev}, PCF_{Ro}, PCF_{Go}, PCF_{Gao} are the theoretical values, the units of these six parameters are kN.

According to Table 3, the linear regression analysis between experimental and theoretical results of the 9 rock samples under 19 cutting conditions is performed. The results are shown in Figure 5, which indicates that all five theoretical models except the Gao Kuidong model performed well. In addition, the model in this paper is the most accurate and has the highest correlation coefficient of 0.9053 while the correlation coefficients of Goktan semi-empirical model, Roxborough model, Evans model, and Gao Kuidong model are 0.8894,

0.8608, 0.8393 and 0.6507, respectively. To compare the lithological tolerance of different theoretical models, PCF data from a wider range of rock samples need to be analyzed.

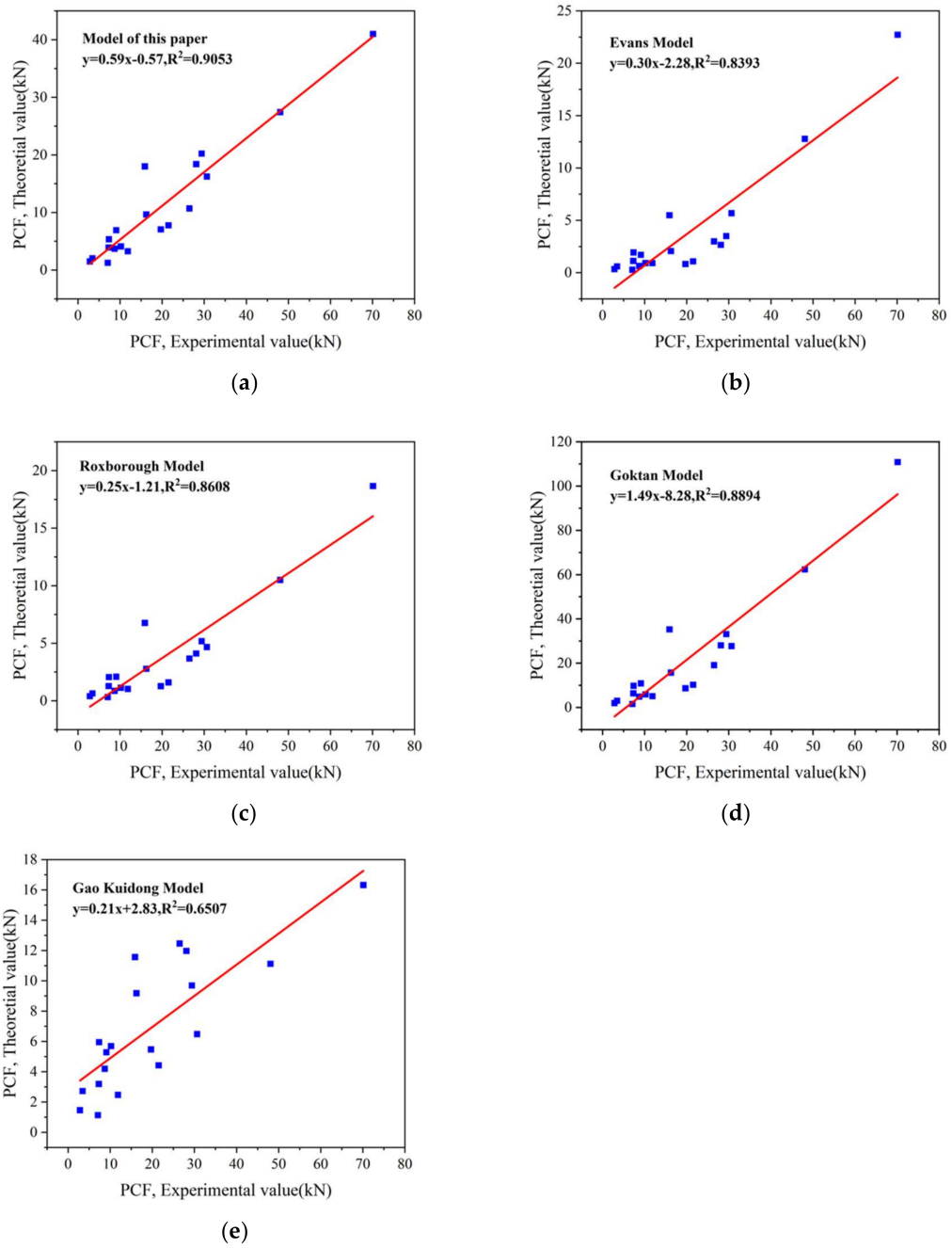

Figure 5. The relationship between theoretical model calculation results and experimental results for the first prediction performance analysis. (**a**) Theoretical model of peak cutting force in this paper; (**b**) Evans model; (**c**) Roxborough model; (**d**) Goktan Semi-empirical model; (**e**) Gao Kuidong model.

In the second analysis, nine additional rock samples were added to the first analysis for assessing the stability of the model in predicting the PCF of complex rock samples. The experimental and theoretical results of these 18 rocks with different properties are analyzed by linear regression under different cutting conditions. The cutting conditions added in the second analysis are listed in Table 4, and the corresponding experimental and theoretical cutting force peaks are recorded in Table 5.

Table 4. The added cutting conditions for the second prediction performance analysis.

Test No.	Rock No.	Pick Type	Installation Angle/°	Cutting Depth/mm	Tip Angle/°	Alloy Head Diameter/mm
10	1(S)	Sandvik 35/80H	57	5/9	80	22
11	2(S)	Sandvik 35/80H	55	10/20	90	22
12	3(S)	Sandvik 35/80H	57	5/9	80	22
13	10(M)	Sandvik 35/80H	57	5/9	80	22
14	11(M)	Sandvik 35/80H	57	5/9	80	22
15	12(M)	Sandvik 35/80H	57	5/9	80	22
16	19(H)	Sandvik 35/80H	57	5/9	80	22
17	20(H)	Sandvik 35/80H	57	5/9	80	22
18	21(H)	Sandvik 35/80H	55	5/10	90	22

Table 5. The added value of PCF obtained by full-scale rock cutting experiments and theoretical models for the second prediction performance analysis.

Test No.	Cut Thickness/mm	PCF_{Ex} [1]	PCF_{this} [1]	PCF_{Ev} [1]	PCF_{Ro} [1]	PCF_{Go} [1]	PCF_{Gao} [1]
10	5	1.33	0.45	0.01	0.03	0.26	0.24
	9	2.18	1.17	0.05	0.08	0.85	0.52
11	10	2.25	1.8	0.66	0.47	2.54	1.32
	20	7.77	4.55	2.63	1.86	10.18	3.32
12	5	2.05	1.05	0.17	0.22	1.18	0.86
	9	4.02	2.74	0.56	0.71	3.82	1.88
13	5	4.4	3.1	0.75	0.88	4.46	/
	9	15.07	8.09	2.43	2.86	14.45	/
14	5	4.74	3.15	1.18	1.15	5.25	/
	9	9.07	8.22	3.83	3.74	17	/
15	10	7.16	3.2	0.92	1.01	4.85	3.7
	15	14.83	8.35	2.97	3.26	15.72	8.11
	20	14.97	4.86	1.12	1.38	7.21	7.68
16	5	26.91	12.65	3.62	4.47	23.37	16.81
	9	12.52	5.66	0.79	1.15	7.21	4.75
17	5	16.3	14.74	2.56	3.74	23.37	10.41
	9	21.98	9.17	1.43	1.37	9.33	7.35
18	5	32.46	23.85	5.74	5.5	37.32	18.53
	10	1.33	0.45	0.01	0.03	0.26	0.24

As shown in Figure 6, a linear regression analysis is performed between the test and theoretical values of the 18 rock samples under 37 cutting conditions in Tables 3 and 5. When the rock samples with K_{Ic} values in the range of 0-2.2 are increased from 9 to 18, the coefficients of determination R^2 of all five models show a small decrease, and the lithological changes appeared to have insignificant effects on the performance of all five predictions.

To further investigate the effect of rock properties on the stability of the PCF calculation model, 9 additional rock samples are added in the third analysis. Their corresponding cutting conditions are listed in Table 6, and the experimental and theoretical results are listed in Table 7.

In the process of rock rupture, the energy required for rock rupture is random and fluctuates due to one or more factors such as rock anisotropy, laminar structure and internal cracks, and its fluctuation increases along with the rock strength. However, the predicted values of PCF for hard rocks by the theoretical model of cut-off force are fixed, so the increase of hard rock samples will inevitably lead to the weakening of the correlation between the theoretical and experimental values, and a good model needs to have high correlation even under such situation.

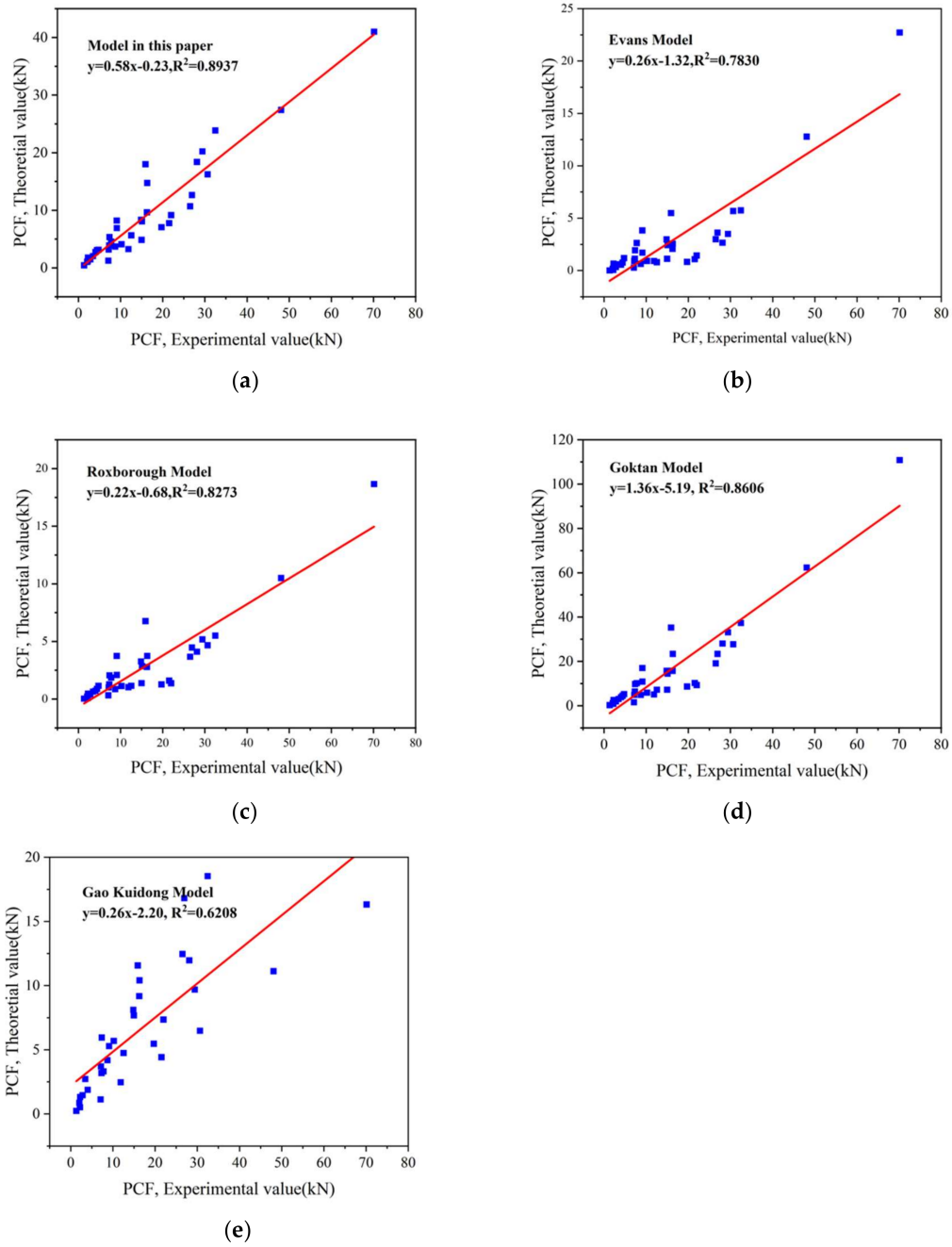

Figure 6. The relationship between theoretical model calculation results and experimental results for the 1st prediction performance analysis. (**a**) Theoretical model of peak cutting force in this paper; (**b**) Evans model; (**c**) Roxborough model; (**d**) Goktan Semi-empirical model; (**e**) Gao Kuidong model.

The peak cut-off force data of 27 rock samples under 61 cutting conditions are analyzed by linear regression, and the fitted lines of the theoretical results and test results of the five models are obtained as shown in Figure 7. When the number of rock samples increased from 18 to 27, the coefficients determination R^2 of the five models showed a significant decrease. When the coefficient of determination R^2 is greater than 0.8, which indicates a strong correlation between the two variables, and when R^2 is less than 0.3, it is considered that there is no correlation between the two variables, otherwise it is considered to have a weak correlation. Figure 7 shows that only the model in this paper has a relatively strong correlation of 0.7792, which is close to 0.8, while the R^2 of the other four models have a relatively large gap to 0.8.

Table 6. The added cutting conditions for the third prediction performance analysis.

Test No.	Rock No.	Pick Type	Installation Angle/°	Cutting Depth/mm	Tip Angle/°	Alloy Head Diameter/mm
19	7(S)	Sandvik 35/80H	57	5/9	80	22
20	8(S)	Sandvik 35/80H	57	5/9	80	22
21	9(S)	Sandvik 35/80H	57	5/9	80	22
22	16(M)	Sandvik 35/80H	57	5/9	80	22
23	17(M)	Sandvik 35/80H	57	5/9	80	22
24	18(M)	Sandvik 35/80H	57	5/9	80	22
		Sandvik 35/80H	55	2/3/5	90	22
		S150-25	50	8	76	25
25	25(H)	S150-25	55	8	76	25
		S150-25	55	4	76	25
		S150-25	45	3/5/7	76	25
26	26(H)	Sandvik 35/80H	57	5/9	80	22
27	27(H)	S150-25	55	4	76	25

Table 7. The added value of PCF obtained by full-scale rock cutting experiments and theoretical models for the third prediction performance analysis.

Test No.	Installation Angle/°	Cut Thickness/mm	PCF_{Ex} [1]	PCF_{this} [1]	PCF_{Ev} [1]	PCF_{Ro} [1]	PCF_{Go} [1]	PCF_{Gao} [1]
19	57	5	3.88	2.45	0.35	0.49	2.88	2.03
	57	9	12.26	6.39	1.12	1.57	9.35	4.44
20	57	5	3.77	2.55	0.54	0.66	3.41	2.7
	57	9	7.22	6.65	1.74	2.13	11.05	5.9
21	57	5	8.72	2.95	0.58	0.74	3.93	/
	57	9	6.53	7.7	1.89	2.39	12.75	/
22	57	5	7.85	4.1	1.83	1.68	7.47	7.35
	57	9	20.15	10.7	5.93	5.45	24.22	16.09
23	57	5	7.33	4.25	1.7	1.65	7.47	/
	57	9	25.82	11.09	5.5	5.34	24.22	/
24	57	2	23.04	4.81	1.04	1.31	6.95	3.03
	57	3	32	12.52	3.36	4.24	22.52	6.64
	57	5	12.52	2.65	0.23	0.24	1.85	2.35
25	55	2	28.72	5.23	0.52	0.55	4.17	4.03
	55	3	33.48	12.02	1.45	1.52	11.59	7.96
	55	5	31.9	21.42	2.99	5.91	11.53	12.24
	50	8	53.56	16.47	2.99	5.91	11.53	12.04
	55	8	9.91	5.2	0.75	1.48	2.88	4.78
	55	4	19	2.88	0.42	0.83	1.62	3.37
	45	3	28.78	9.14	1.17	2.31	4.5	6.66
	45	5	29.47	17.33	2.29	4.52	8.83	10.42
	45	7	14.83	5.63	0.53	1.21	2.85	18.74
26	57	5	23.25	10.76	1.66	2.43	15.21	9.43
	57	9	48.7	28.04	5.37	7.86	49.29	20.65
27	55	4	3.88	2.45	0.35	0.49	2.88	2.03

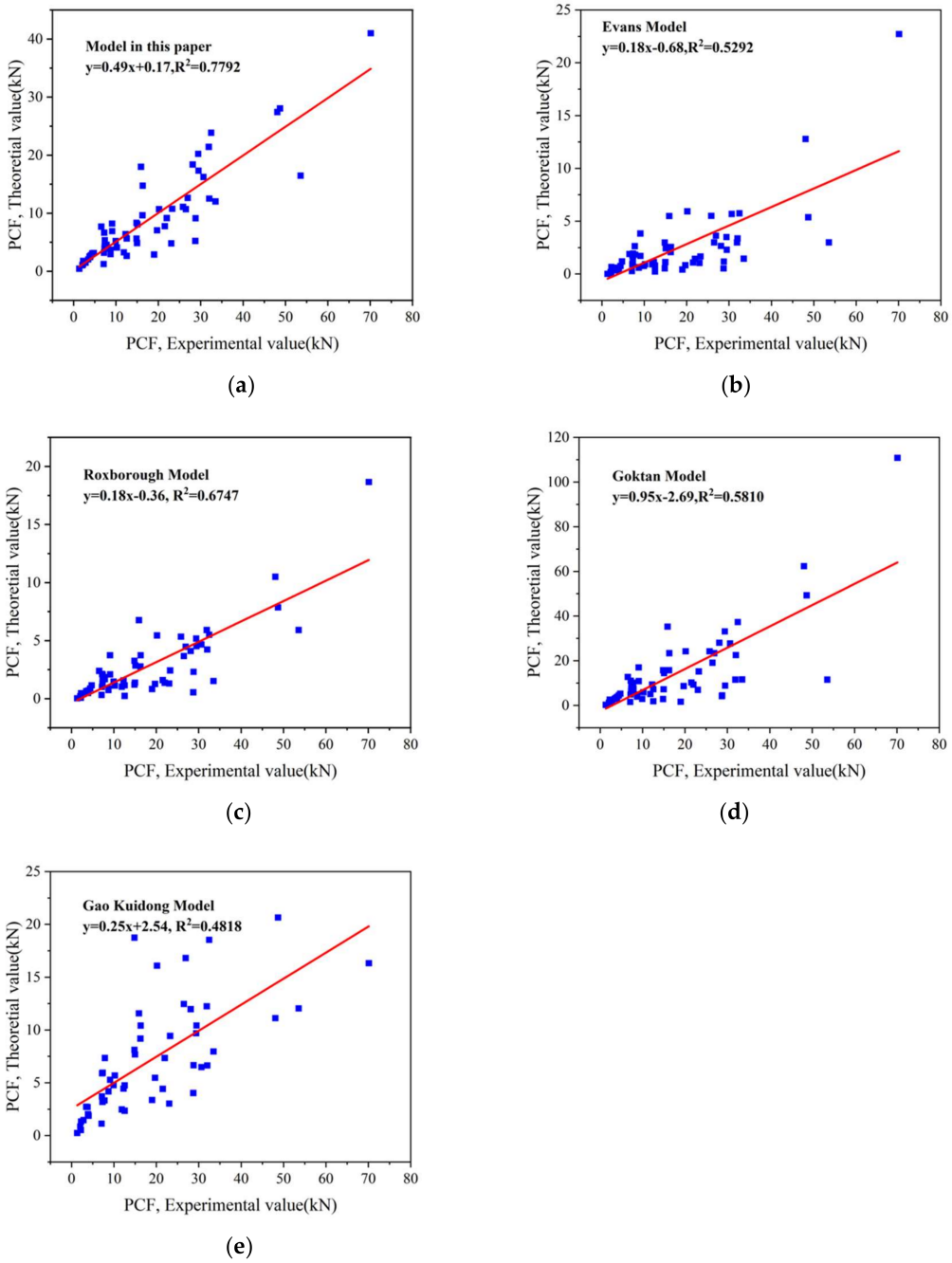

Figure 7. The relationship between theoretical model calculation results and experimental results for the first prediction performance analysis. (**a**) Theoretical model of peak cutting force in this paper; (**b**) Evans model; (**c**) Roxborough model; (**d**) Goktan Semi-empirical model; (**e**) Gao Kuidong model.

Table 8 and Figure 8 reflect the variation of the coefficient of determination for each model in the three analyses. In the three analyses, the number of rock samples gradually increased from 9 to 27, and the proposed model in this paper always maintains the strongest linear correlation compared with other models. Besides, when the number of rock samples increases, as a result of the large fluctuation of PCF when cutting hard rocks, the correlation of all five theoretical models showed a decreasing trend, but the correlation of this model decreases the least after three analyses, and the R^2 only decreases by 13.93% while the other models decrease by more than 21.62%.

Table 8. Variation of the coefficient of determination in the three analyses.

Analysis No.	No. of Rock Samples	No. of Data	R^2_{this} [1]	R^2_{Ev} [1]	R^2_{Ro} [1]	R^2_{Go} [1]	R^2_{Gao} [1]
1st	9	19	0.9053	0.8393	0.8608	0.8894	0.6507
2nd	18	37	0.8937	0.7830	0.8273	0.8606	0.6208
3rd	27	61	0.7792	0.5292	0.6747	0.5810	0.4818

[1] R^2_{this}, R^2_{Ev}, R^2_{Ro}, R^2_{Go} *and* R^2_{Gao} are the coefficient of determination for the model of this paper, Evans model, Roxborough model, Goktan semi-empirical model and Gao Kuidong model, respectively.

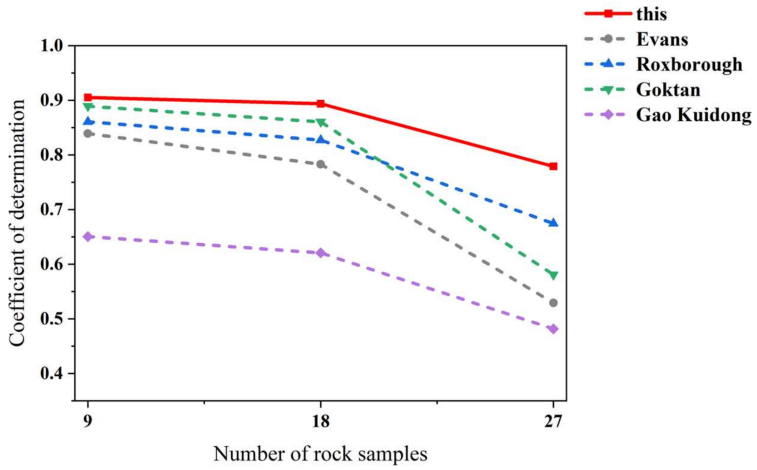

Figure 8. Line graph reflecting the change in the coefficient of determination in the three analyses.

In addition, the root mean square error (RMSE) between the theoretical results and the experimental results is calculated separately to evaluate the accuracy of the theoretical model prediction. As shown in Table 9 and Figure 9, for 27 rock samples the RMSE of the theoretical model proposed in this paper is the lowest of 11.74 followed by the Goktan semi-empirical model with RMSE of 11.81, while Evans model has the highest RMSE of 19.10.

Table 9. Root mean square error of each theoretical model.

Analysis No.	No. of Rock Samples	No. of Data	$RMSE^2_{this}$ [1]	$RMSE^2_{Ev}$ [1]	$RMSE^2_{Ro}$ [1]	$RMSE^2_{Go}$ [1]	$RMSE^2_{Gao}$ [1]
1st	9	19	11.47	19.90	20.33	11.88	18.43
2nd	18	37	9.33	16.57	16.77	9.15	14.55
3rd	27	61	11.74	19.10	18.78	11.81	16.20

[1] R^2_{this}, R^2_{Ev}, R^2_{Ro}, R^2_{Go} *and* R^2_{Gao} are the coefficient of determination for the model of this paper, Evans model, Roxborough model, Goktan semi-empirical model and Gao Kuidong model, respectively, the units of these five parameters are kN.

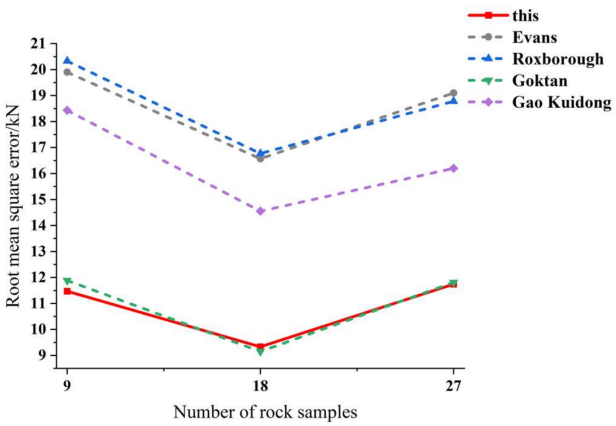

Figure 9. Line graph reflecting the change in the root mean square error in the three analyses.

According to Figure 9, the root mean square error of the model proposed in this paper is the smallest among the five models in most cases, indicating that the deviation between the predicted and experimental values of this model is the smallest and the prediction results are more accurate.

In conclusion, through linear regression analysis and root mean square error analysis, compared with existing models, the model proposed in this paper has the most accurate performance in predicting the PCF of complex rock samples. In addition, it has the highest lithological tolerance which presents the best stability in prediction of a large number of complex lithologic samples.

4. Conclusions

In this paper, peak cutting force estimation with improved projection profile method is proposed considering conical picks' structural and installation parameters, thus improving the theoretical prediction accuracy of the PCF as well as the capability of lithological tolerance for rock samples of complex lithology. The following conclusions are drawn from the present study.

(1) The improved projection profile method can cover the mechanical property of alloy head and conical pick body in rock fracture process, which is more suitable for rock fracturing capacity prediction than the existing method which only considers alloy head and ignores the role of conical pick body.
(2) In the linear regression analysis and root-mean-square error analysis of 27 rock samples, compared with the Evans model, the correlation coefficient is increased by 47.24% and the root mean square error is reduced by 38.53%, which provides the basis of quantitative accuracy in rock breaking capacity prediction.
(3) Compared with the other four models, the prediction performance of this method is the most stable when the rock type increases and the lithology changes. The decrease of correlation coefficient R^2 is less than 13.93% when the rock sample increases, while other models decrease by more than 21.62%. The reliability and stability of PCF prediction provide a technical basis for the subsequent optimal design of conical pick parameters which consider lithological tolerance.

Author Contributions: Conceptualization, M.D., Q.H. and Y.H.; methodology, M.D.; software, L.S.; validation, M.D. and L.S.; formal analysis, C.W.; investigation, C.W.; resources, X.L.; data curation, M.D.; writing—original draft preparation, L.S.; writing—review and editing, M.D.; visualization, C.W.; supervision, Q.H.; project administration, Q.H.; funding acquisition, Y.H. and X.L. All authors have read and agreed to the published version of the manuscript.

Funding: This research was funded by the National Natural Science Foundation of China (No. 51575201).

Institutional Review Board Statement: Not applicable.

Informed Consent Statement: Not applicable.

Data Availability Statement: Exclude this statement.

Acknowledgments: This work was financially supported by the National Natural Science Foundation of China (No. 51575201).

Conflicts of Interest: The authors declare no conflict of interest.

Nomenclature

PCF	The Peck Cutting Force
UCS	The Uniaxial Compressive Strength
BTS	The Brazilian Tensile Strength
RMSE	The Root Mean Square Error

α	the half tip angle
α_1	the taper angle of pick body
r	the radius of alloy head
β	the front angle
γ	the installation angle
d	the cutting depth
a	the long semi-axis
b	the short semi-axis
θ_0	the semi-envelope angle
θ	the position angle
λ	the radius of the simplified circle
k_1	the correction coefficients
k_2	the correction coefficients
k_3	the correction coefficients
ρ_S	the surface energy density
U_0	the energy given by the truncation process
G_S	the energy for new surface
δ	the initial crack size
μ	the rock Poisson's ratio
E	the rock modulus of elasticity
K_{Ic}	the rock type I fracture toughness
ϕ	the horizontal rupture angle
K	the constant related to pick shape and cutting angle
ψ'	the vertical rupture angle

References

1. Evans, I. A theory of the basic mechanics of coal ploughing. In *Proceedings of the International Symposium on Mining Research*, 2nd ed.; Clark, G.B., Ed.; Pergamon Press: Oxford, UK, 1961; pp. 761–798.
2. Evans, I. Theory of the cutting force for point-attack picks. *Int. J. Min.* **1984**, *2*, 63–71. [CrossRef]
3. Roxborough, F.F.; Liu, Z.C. Theoretical considerations on pick shape in rock and coal cutting. In Proceedings of the Sixth Underground Operator's Conference, Kalgoorlie, Australia, 13–14 November 1995.
4. Goktan, R.M. A suggested improvement on Evans' cutting theory for conical bits. In Proceedings of the Fourth International Symposium on Mine Mechanization and Automation, Brisbane, Australia, 6–9 July 1997.
5. Goktan, R.M.; Gunes, N. A semi-empirical approach to cutting force prediction for point-attack picks. *J. S. Afr. Inst. Min. Metall.* **2005**, *105*, 257–263.
6. Nishimatsu, Y. The mechanics of the rock cutting. *Int. J. Rock Mech. Min. Sci.* **1972**, *9*, 261–271. [CrossRef]
7. Bilgin, N.; Demircin, M.A. Dominant rock properties affecting the performance of conical picks and the comparison of some experimental and theoretical results. *Int. J. Rock Mech. Min. Sci.* **2006**, *43*, 139–156. [CrossRef]
8. Tiryaki, B.; Boland, J.N. Empirical models to predict mean cutting forces on point-attack pick cutters. *Int. J. Rock Mech. Min. Sci.* **2010**, *47*, 858–864. [CrossRef]
9. Bao, R.H.; Zhang, L.C. Estimating the peak indentation force of the edge chipping of rocks using single point-attack pick. *Rock Mech. Rock Eng.* **2011**, *44*, 339–347. [CrossRef]
10. Kuidong, G.; Du Changlong, J.H. A theoretical model for predicting the Peak Cutting Force of conical picks. *Fract. Struct. Integr.* **2014**, *8*, 43–52. [CrossRef]
11. Li, X.F.; Wang, S. Numerical simulation of rock breakage modes under confining pressures in deep mining: An experimental investigation. *IEEE Access* **2016**, *4*, 5710–5720. [CrossRef]
12. Li, X.F.; Wang, S. Numerical simulation of rock fragmentation during cutting by conical picks under confining pressure. *Comptes Rendus. Mécanique* **2017**, *345*, 890–902. [CrossRef]
13. Li, X.F.; Wang, S. A theoretical model for estimating the peak cutting force of conical picks. *Exp. Mech.* **2018**, *58*, 709–720. [CrossRef]
14. Li, X.F.; Wang, S. A study on drum cutting properties with full-scale experiments and numerical simulations. *Measurement* **2018**, *114*, 25–36. [CrossRef]
15. Li, X.F.; Wang, S. Investigation on the influence mechanism of rock brittleness on rock fragmentation and cutting performance by discrete element method. *Measurement* **2018**, *113*, 120–130.
16. Li, H.S.; Liu, S.Y. Numerical simulation on interaction stress analysis of rock with conical picks. *Tunn. Undergr. Space Technol.* **2019**, *85*, 231–242. [CrossRef]
17. Wang, S.; Huang, L. Analysis of rockburst triggered by hard rock fragmentation using a conical pick under high uniaxial stress. *Tunn. Undergr. Space Technol.* **2020**, *96*, 103195. [CrossRef]

18. Wang, S.; Yu, T.A.N.G. Analyses and predictions of rock cuttabilities under different confining stresses and rock properties based on rock indentation tests by conical pick. *Trans. Nonferrous Met. Soc. China* **2021**, *31*, 1766–1783. [CrossRef]
19. Wang, S.; Sun, L. Experimental investigation of cuttability improvement for hard rock fragmentation using conical cutter. *Int. J. Geomech.* **2021**, *21*, 06020039. [CrossRef]
20. Wang, S. Experimental investigation and theoretical analysis of indentations on cuboid hard rock using a conical pick under uniaxial lateral stress. *Geomech. Geophys. Geo-Energy Geo-Resour.* **2022**, *8*, 34. [CrossRef]
21. Gao, K.D.; Du, C.L.; Liu, X. Study on the variation law of pick teeth installation angle and half taper angle with cut-off depth. *Coal Sci. Technol.* **2011**, *39*, 93–96.
22. Wang, L.P.; Jiang, B.S.; Zhang, Q. Calculation of peak cut-off force for asymmetric cut-off slot of pick-type cut-off teeth. *J. Coal* **2016**, *41*, 2876–2882.
23. Roxborough, F.F.; King, P.; Pedroncelli, E.J. Tests on the cutting performance of a continuous miner. *J. S. Afr. Inst. Min. Metall.* **1981**, *81*, 9–25.
24. Roxborough, F.F.; Pedroncelli, E.J. Practical evaluation of some coal-cutting theories using a continuous miner. *Min. Eng.* **1982**, *142*.
25. Yang, X.; Sun, L.; Song, J. Study on the Effect of Bond Strength on the Failure Mode of Coarse-Grained Sandstone in Weakly Cemented Stratum. *Minerals* **2022**, *12*, 55. [CrossRef]
26. Liu, D.; Zhang, Y.; Zhou, A. The Kaolinite Crystallinity and Influence Factors of Coal-Measure Kaolinite Rock from Datong Coalfield, China. *Minerals* **2022**, *12*, 54. [CrossRef]
27. Hu, X.; Zhang, M.; Xu, W. A Dynamic Coupled Elastoplastic Damage Model for Rock-like Materials Considering Tension-Compression Damage and Pressure-Dependent Behavior. *Minerals* **2022**, *12*, 851. [CrossRef]
28. Ren, C.; Xu, J.; Xu, J. Coal–Rock Cutting Sound Denoising Based on Complete Ensemble Empirical Mode Decomposition with Adaptive Noise and an improved Fruit Fly Optimization Algorithm. *Machines* **2022**, *10*, 412. [CrossRef]